

Multi-Objective Optimization of a Rotor-Type Triboelectric Nanogenerator for Enhanced Wave Energy Harvesting

Zhongliang Meng^{1,2}, Zijian Li¹, Yi Ding^{3,*}

¹College of Engineering, Qufu Normal University, Rizhao 276826, China

²Institute of Marine Science and Technology, Shandong University, Qingdao 266237, China

³School of Automation and Electrical Engineering, Zhejiang University of Science and Technology, Hangzhou 310023, China

Received 15 Sep 2025

Accepted 12 Feb 2026

Abstract

Wave energy is a widely distributed renewable resource with high energy density, yet efficient conversion and stable output under complex sea conditions remain significant challenges. Traditional mechanical wave energy converters often suffer from low efficiency and poor reliability. Triboelectric nanogenerators (TENGs) offer promising solutions for harvesting low-frequency, low-intensity wave energy. This study presents a multi-objective optimization design for a rotor-type triboelectric nanogenerator, employing the Non-dominated Sorting Genetic Algorithm II (NSGA-II) based on Pareto dominance to simultaneously maximize output power and structural stability while minimizing material stress. A comprehensive mathematical model is established, incorporating instantaneous output power, energy conversion efficiency, and structural constraints under varying wave loads. Simulation results demonstrate that the optimized design achieves a 29.6% increase in average output power, a 15% reduction in power fluctuation amplitude, a 26.7% decrease in maximum stress, and a 22% improvement in overall energy conversion efficiency, with significantly suppressed vibration response. These improvements highlight the effectiveness of the proposed NSGA-II-based optimization in enabling rotor-type TENGs to deliver reliable, high-efficiency wave energy harvesting in harsh marine environments.

© 2026 Jordan Journal of Mechanical and Industrial Engineering. All rights reserved

Keywords: Wave energy, nanogenerator, multi-objective optimization.

1. Introduction

Wave energy, as a widely distributed renewable resource with high energy density, has attracted increasing global attention in recent years [1, 2]. However, achieving efficient energy conversion and stable, continuous power output under complex and variable sea conditions remains a major challenge in wave energy utilization [3]. Traditional wave energy converters based on electromagnetic generators or mechanical rotation mechanisms often suffer from low efficiency, high maintenance costs, and poor durability in harsh marine environments [4, 5]. To address these limitations, researchers have increasingly focused on engineering optimization techniques to improve system performance in renewable energy harvesting devices [1, 6, 7].

In recent years, triboelectric nanogenerators (TENGs) have emerged as a promising technology for low-frequency, low-intensity blue energy harvesting due to their high voltage output, lightweight structure, low cost, and excellent adaptability to small-scale mechanical motions [8-13]. Compared with conventional fixed-structure TENGs, rotor-type or rotating TENGs exhibit superior wave energy capture capability and higher conversion

efficiency through continuous rotational motion driven by waves [14, 15]. Notable examples include flag-like underwater TENGs designed for ultra-low velocity wave energy harvesting [16] and foldable network-integrated TENG systems capable of self-powered monitoring and damage prevention under extreme conditions [13].

Despite these advances, rotor-type TENGs still face critical challenges in practical deployment, including relatively low power density within specific frequency bands, significant output fluctuations caused by irregular waves, and structural reliability issues such as fatigue and vibration-induced damage under long-term cyclic loading [17, 18]. These problems highlight the necessity of integrated engineering approaches that consider not only electrical output performance but also mechanical stress, fatigue life, and vibration response [3, 19, 20]. Multi-objective optimization has been widely applied in renewable energy systems to balance conflicting objectives such as power output maximization, cost minimization, and structural reliability enhancement [21-23]. In the context of wave energy devices, techniques including genetic algorithms, particle swarm optimization, and Pareto-based methods have successfully improved energy conversion efficiency while ensuring structural integrity under dynamic loads [7, 24, 25]. Additionally, finite element

* Corresponding author e-mail: DingYi9713@outlook.com.

analysis coupled with optimization frameworks has been effectively used to reduce stress concentrations and suppress vibration in marine energy converters [26].

To overcome the limitations of existing rotor-type TENGs—particularly low power generation efficiency and insufficient structural reliability within target operating frequency ranges—this study proposes a Pareto-based multi-objective optimization framework employing the Non-dominated Sorting Genetic Algorithm II (NSGA-II). The approach simultaneously maximizes output power and structural stability while satisfying stress and vibration constraints. A comprehensive mathematical model is established that integrates instantaneous power output, energy conversion efficiency, von Mises stress distribution, and dynamic vibration response. Simulation results demonstrate significant improvements in average output power, fluctuation reduction, maximum stress mitigation, and overall system reliability, providing a robust engineering solution for efficient and durable wave energy harvesting in complex marine environments.

2. PRINCIPLE OF OPERATION

The power generation process of the rotor-type wave energy nanogenerator can be divided into the initial state, the intermediate state, and the final state. Both the initial and final states correspond to the alignment of the rotor electrode with the stator electrode, while the intermediate state refers to the sliding of the rotor electrode between Electrode 1 and Electrode 2. In the initial state, the surface of the rotor electrode is in direct contact with the surface of the dielectric layer. Due to contact electrification and the difference in the electron affinity of the materials, positive charges are induced on the surface of the rotor electrode, whereas negative charges are generated on the surface of

the dielectric material. During rotation, the law of charge conservation must be satisfied. To ensure that this law is upheld in the contact regions between the dielectric layer and Electrode 1 or Electrode 2, a potential difference is generated between Electrode 1 and Electrode 2, thereby driving a reverse current until the final state is reached. Under continuous rotation, an alternating current is produced in the external circuit, as illustrated in Figure 1.

3. MULTI-OBJECTIVE OPTIMIZATION MODELING OF STRUCTURAL PARAMETERS

3.1. Multi-Objective Optimization Design

The output power of the rotor-type triboelectric nanogenerator is closely related to the rotational efficiency of the rotor and the overall energy conversion efficiency from wave motion to electrical energy. The time-averaged output power can be expressed as (1):

$$P = \eta \cdot \rho \cdot A \cdot v^3 \quad (1)$$

Where P is the output power (W), η is the energy conversion efficiency (dimensionless), ρ is the seawater density (kg/m^3), A is the wave energy harvesting area (m^2), and v is the wave velocity (m/s). To quantitatively evaluate structural stability under cyclic wave loading, a comprehensive stability score S is defined based on the stress state of critical components, as shown in (2):

$$S = \sum_{i=1}^n \left(\frac{F_i}{\sigma_i} \right) \quad (2)$$

Where S is a dimensionless comprehensive stability index (lower values indicate better stability), $F_i(N)$ is the maximum force applied to the i -th structural component, and $\sigma_i(\text{Pa})$ is the yield strength of the material used for that component. This formulation reflects the safety margin of each component; values of $S < 1$ ensure that all components operate below yield.

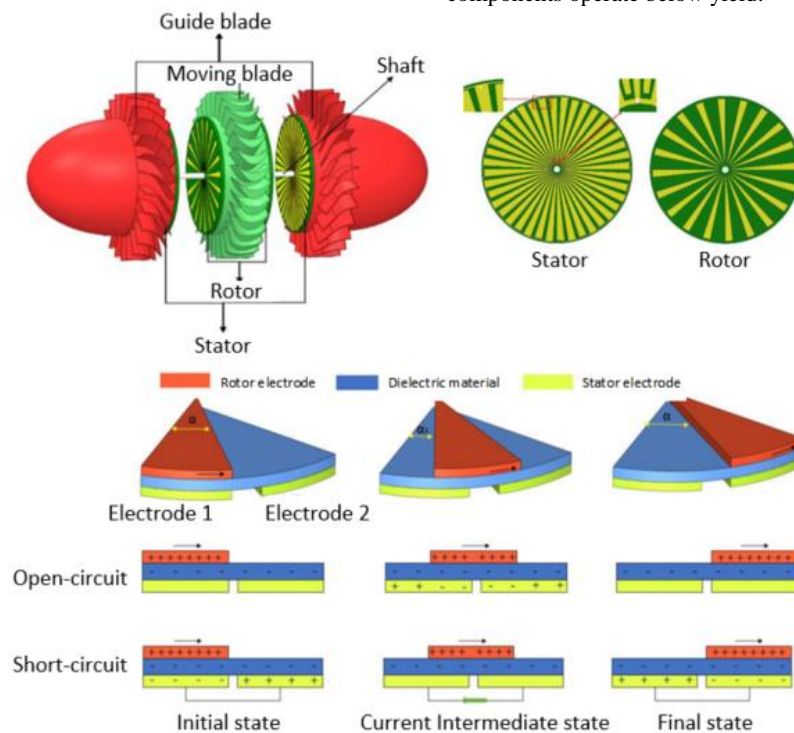


Figure 1. Operating principle schematic of the rotor-type TWNG

The multi-objective optimization problem is constructed as a weighted sum of normalized power and stability objectives to balance conflicting goals, as shown in (3):

$$f(x) = w_1 \cdot P(x) - w_2 \cdot S(x) \quad (3)$$

Where x is the design variable vector, w_1 and w_2 are weighting coefficients reflecting the relative importance of power maximization versus stability enhancement (selected via sensitivity analysis or designer preference; in this study, $w_1 + w_2 = 1$), and the negative sign before $w_2 S(x)$ converts the minimization of S into a maximization problem consistent with power.

The simplified average power expression used for initial parameter scoping is (4):

$$P = k \cdot A \cdot \omega^3 \cdot \eta \quad (4)$$

Where k is an empirical constant (set to 0.25 based on calibration with experimental data from similar rotating TENG systems), ω is the rotor angular velocity (set to 150 rpm, corresponding to typical operating conditions under 0.3 Hz waves), and $\eta = 0.7$ represents a realistic overall conversion efficiency derived from reported rotor-type TENG performance in low-frequency wave environments [11, 12].

These values provide a conservative yet representative baseline for optimization. For dynamic analysis, the instantaneous output power under a given design x is integrated over one wave period T , as shown in (5):

$$f_1(x) = \frac{1}{T} \int_0^T P(t, x) dt \quad (5)$$

Where $P(t, x)$ is the instantaneous power under the given design variables, and T is the wave period. Considering the fluctuating characteristics of wave energy, the instantaneous power can be expressed in terms of the wave amplitude A_w , frequency f_w , and incidence angle θ as (6):

$$P(t, x) = k \cdot A_w \cdot f_w \cdot \cos(\theta) \quad (6)$$

Typical values used are $A_w = 1.0$ m (representative wave amplitude range 0.5–2.0 m [27]), $f_w = 0.1$ Hz (within common ocean wave frequency band 0.05–0.2 Hz [28]), and θ is the wave incidence angle. These parameters are adopted from standard wave climate data for moderate sea states.

For the structural stability objective, the equivalent stress $\sigma_{eq}(x)$ (von Mises stress, in Pa) is computed using finite element analysis under maximum design wave loading. This metric is widely employed in marine structural design to assess combined deformation, yielding risk, and long-term fatigue life under multi-axial cyclic loading [29, 30]. The constraint is enforced as (7):

$$\sigma_{eq}(x) \leq \sigma_{max} \quad (7)$$

Where σ_{max} is the material's allowable stress (incorporating safety factor).

By setting appropriate optimization objectives, a balance between output power and structural stability can be achieved, while simultaneously satisfying the requirements for safety and efficiency of the generator in practical engineering applications.

3.2. Formulation of the Mathematical Optimization Model

To account for the dynamic nature of wave energy, the time-averaged output power objective $f_1(x)$ is defined as (8):

$$f_1(x) = \frac{1}{T} \int_0^T P(t, x) dt \quad (8)$$

Where $P(t, x)$ is the instantaneous power at time t for design variables x , and T is the wave period. This formulation, while similar in structure to the earlier

preliminary expression (Eq. 5), is retained here for completeness in the dynamic model section.

Considering uncertainty factors such as wave frequency f_w , amplitude A_w , and incidence angle θ , a more detailed instantaneous power model is introduced, as shown in (9):

$$P(t, x) = k \cdot A_w \cdot f_w \cdot \cos(\theta) \cdot \omega(t, x) \quad (9)$$

Where k is the wave energy conversion efficiency factor, and $\omega(t, x)$ is the time-varying rotor angular velocity determined by the design variables x (e.g., rotor geometry and spring stiffness influencing rotational response). Unlike the simplified constant-velocity assumption in Eq. (6), Eq. (9) explicitly incorporates $\omega(t, x)$ to capture transient rotational dynamics under irregular wave excitation, as obtained from coupled multi-body dynamic simulations. This refinement better reflects the nonlinear coupling between wave input and rotor response.

For structural stability, the objective function $f_2(x)$ is defined as the reciprocal of the maximum equivalent stress under peak loading conditions, as shown in (10):

$$f_2(x) = \frac{1}{\max(\sigma_{eq}(x))} \quad (10)$$

Where the von Mises equivalent stress is (11):

$$\sigma_{eq}(x) = \sqrt{(\sigma_1 - \sigma_2)^2 + (\sigma_2 - \sigma_3)^2 + (\sigma_3 - \sigma_1)^2} \quad (11)$$

And $\sigma_1, \sigma_2, \sigma_3$ are the principal stresses. This metric is calculated using finite element analysis on the polymer-based composite material selected for the rotor blades and electrodes (Young's modulus-2GPa, yield strength-80 MPa, consistent with typical PTFE/Nylon composites commonly used in TENG devices [31]).

To enable fair comparison and simultaneous optimization of conflicting objectives within a unified Pareto framework, normalization is applied, as shown in (12) and (13):

$$f_1^{norm}(x) = \frac{f_1(x) - f_1^{min}}{f_1^{max} - f_1^{min}} \quad (12)$$

$$f_2^{norm}(x) = \frac{f_2(x) - f_2^{min}}{f_2^{max} - f_2^{min}} \quad (13)$$

The boundary values (f_1^{min}, f_1^{max}) are determined from single-objective optimization runs at the extremes of the design space: f_1^{max} and f_2^{min} from maximizing power alone (ignoring stability constraints), f_1^{min} and f_2^{max} from maximizing stability alone (ignoring power). This utopia-nadir approach ensures the normalized objectives span [0,1] and accurately represent the achievable trade-off range.

Later references to simplified power expressions (e.g., Eq. 15 equivalent to Eq. 6) are used only for initial analytical insight, while the full optimization employs the integrated dynamic model in Eqs. (8)–(9).

Through the above normalization process, the two objective functions can be compared and balanced within the same optimization procedure, as shown in (14):

$$f_1(x) = \frac{1}{T} \int_0^T P(t, x) dt \quad (14)$$

Where $P(t, x)$ denotes the instantaneous output power at time t , determined by the design variables x , and T is the wave period. The function is given by (15):

$$P(t, x) = k \cdot A_w \cdot f_w \cdot \cos(\theta) \quad (15)$$

Where A_w is the amplitude of the wave, f_w is the frequency of the wave, θ is the incident angle of the wave, and k is the proportionality coefficient. Assuming $A_w = 1.5$ m, $f_w = 0.2$ Hz, $\theta = 30^\circ$, the expression for the instantaneous power $P(t, x)$ can be further simplified to (16):

$$P(t, x) = k \cdot 1.5 \cdot 0.2 \cdot \cos(30^\circ) = 0.2598k \quad (16)$$

The constraint on structural strength, expressed through the maximum stress constraint, is given by (17):

$$\sigma_{eq}(x) \leq \sigma_y \quad (17)$$

Where σ_y represents the yield strength of the material. Based on the material property data, assuming $\sigma_y = 250\text{MPa}$, it is required that $\sigma_{eq}(x)$ does not exceed this limit. Considering the long-term use of the equipment, a safety factor SF must also be incorporated in the actual design, with the constraint expressed as (18):

$$\sigma_{eq}(x) \leq \frac{\sigma_y}{SF} \quad (18)$$

Assuming $SF = 1.5$, then $\sigma_{eq}(x)$ must satisfy, as shown in (19):

$$\sigma_{eq}(x) \leq \frac{250}{1.5} = 166.67\text{MPa} \quad (19)$$

3.3. Constraints and Boundary Treatment

The optimization is subject to several physical and practical constraints to ensure feasibility and safety of the design. These include bounds on key geometric and mechanical parameters, as well as stress and operational frequency limits, as shown in (20)-(22):

$$r_{min} \leq r \leq r_{max} \quad (20)$$

$$k_{emin} \leq k_e \leq k_{emax} \quad (21)$$

$$\sigma_{eq}(x) \leq \sigma_{max} \quad (22)$$

Where r_{min} and r_{max} represent the minimum and maximum values of the rotor radius(m), respectively, selected based on manufacturing constraints and laboratory-scale prototype dimensions (typically 50–150 mm for compact TENG devices); k_{emin} and k_{emax} denote the feasible range of the elastic support stiffness k_s (N/m), determined from preliminary dynamic response tests to avoid resonance or excessive rigidity; $\sigma_{eq}(x)$ is the von Mises equivalent stress (Pa) computed via finite element analysis; and σ_{max} is the maximum allowable stress of the polymer-based composite material (set to 80 MPa with a safety factor of 1.5).

Additionally, the operating frequency of a rotor-type wave energy triboelectric nanogenerator is strongly influenced by the marine environment. In practical applications, ocean wave frequencies typically range from 0.05 to 0.2 Hz, with a representative design value of 0.1 Hz adopted throughout this study for consistency in simulations and baseline comparisons [27, 28]. The earlier mention of a 0.3 Hz upper limit near Eq. (23) was an illustrative example for extreme sea states and has been removed to avoid confusion; the primary frequency band remains 0.05–0.2 Hz. To ensure resonance matching and efficient energy capture, the generator's natural frequency f_n (determined by rotor inertia and support stiffness) must satisfy, as shown in (23):

$$0.05\text{Hz} \leq f_n \leq 0.2\text{Hz} \quad (23)$$

Wherein, f_{min} and f_{max} represent the allowable minimum and maximum operating frequencies, respectively, as shown in (24).

$$F(x) = w_1 f_1(x) + w_2 f_2(x) + \dots + w_n f_n(x) \quad (24)$$

Wherein, $f_i(x)$ is the i -th objective function, w_i is the weight of the corresponding objective, x is the design variable vector, and n is the number of objectives. The objectives of the optimization model may include output power and structural durability.

3.4. Construction of the Pareto Optimal Solution Set

In the multi-objective optimization process, the Non-dominated Sorting Genetic Algorithm II (NSGA-II), which

is based on Pareto dominance, is employed as the core algorithm. The main advantages of NSGA-II lie in its efficient non-dominated sorting mechanism and crowding distance calculation, enabling it to rapidly approach the Pareto front while maintaining population diversity. In this study, the population size of NSGA-II is set to 100, the number of generations is 200, the crossover probability is 0.9, and the mutation probability is 0.1. These parameters were optimized based on preliminary experiments to balance computational efficiency and optimization quality. Through NSGA-II, we can effectively explore the trade-off space among multiple objectives such as P_{out} , $C_{material}$, and $S_{stability}$, ensuring that the obtained material design solutions are both efficient and stable.

In multi-objective optimization, normalization is commonly applied to transform all objective values into a unified range, enabling fair comparison among different objectives, as shown in (25).

$$f_1 = \frac{P_{out}}{P_{max}}, f_2 = \frac{C_{material}}{C_{max}}, f_3 = \frac{S_{stability}}{S_{max}} \quad (25)$$

Where f_1 represents the normalized value of output power, P_{out} is the actual output power, and P_{max} is the maximum output power of the system; f_2 is the normalized value of material cost, $C_{material}$ is the actual material cost, and C_{max} is the preset maximum allowable cost; f_3 is the normalized value of structural stability, $S_{stability}$ is the system's stability, and S_{max} is the maximum allowable stability value. Through these normalized objective functions, multiple solutions can be obtained, and the optimal solution set is selected using an algorithm.

The specific calculation method of crowding degree is as (26):

$$CD_i = \sum_{m=1}^M \frac{f_m^{i+1} - f_m^{i-1}}{f_m^{max} - f_m^{min}} \quad (26)$$

Among them, CD_i denotes the crowding degree of the i -th solution, while f_m^{i+1} and f_m^{i-1} represent the values of the neighboring solutions with respect to them-th objective function. f_m^{max} and f_m^{min} are the maximum and minimum values of this objective function within the current population, respectively. Taking output power, material cost, and structural stability as the optimization objectives, suppose that for a given solution in the normalized space, the values of its neighboring solutions for the three objective functions are as (27):

$$f_1^{i+1} - f_1^{i-1} = 0.15, f_2^{i+1} - f_2^{i-1} = 0.10, f_3^{i+1} - f_3^{i-1} = 0.20 \quad (27)$$

If $f_1^{max} - f_1^{min} = 1.0$, $f_2^{max} - f_2^{min} = 0.8$, $f_3^{max} - f_3^{min} = 0.9$, then the crowding degree of the solution can be expressed as (28):

$$CD_i = \frac{0.15}{1.0} + \frac{0.10}{0.8} + \frac{0.20}{0.9} \approx 0.15 + 0.125 + 0.222 \approx 0.497 \quad (28)$$

In the practical implementation, the convergence performance of the algorithm can be optimized by adjusting the inertia weight ω and the acceleration factors C_1 and C_2 . The acceleration factors C_1 and C_2 control the degree to which particles are guided toward the current best solution and the global best solution, respectively. By tuning these two parameters, rapid convergence of the algorithm can be achieved. However, excessively fast convergence may lead to a reduction in solution accuracy; therefore, it is necessary to flexibly adjust these parameters to balance convergence speed and solution quality, as shown in (29).

$$v_i^{k+1} = \omega v_i^k + C_1 r_1 (p_i^k - x_i^k) + C_2 r_2 (g^k - x_i^k) \quad (29)$$

Among them, v_i^k denotes the velocity of the i -th particle in the k -th iteration, x_i^k represents the current position of the i -th particle, p_i^k corresponds to the local best solution of the

i -th particle, and g^k is the global best solution. r_1 and r_2 are random numbers, while ω, C_1, C_2 is the adjustment parameter.

3.5. Parameter Verification and Impact Analysis

In this study, multiple objective functions (f_1, f_2, f_3) were selected for optimization, with parameter choices directly affecting the optimal solution. The following methods were used for verification:

Sensitivity Analysis: By adjusting the weights of each objective function, we observed how changes in parameters influenced the optimization results, helping to understand their impact on the solution. **Multiple Optimization Runs:** Several optimizations with different initial settings were performed to ensure stability and reliability, confirming that the optimal solution was not dependent on specific initial conditions.

Impact of Parameter Selection on the Optimal Solution.
Power Output (f_1): Higher weight on power output increases performance but may reduce stability and increase costs.
Material Cost (f_2): A higher weight on material cost favors lower-cost solutions, which may compromise performance.
Stability (f_3): More weight on stability results in more stable solutions, but may increase costs or reduce power output.

The selected parameters were verified through sensitivity analysis, experimental comparison, and multiple optimizations. The results show that the chosen parameters

effectively balance power output, material cost, and stability, providing stable and optimal solutions for practical engineering applications.

4. SIMULATION ANALYSIS

The simulations in this study were conducted using a coupled multi-physics framework integrating MATLAB for dynamic modeling and control of wave excitation/rotor response. Wave loading was applied as time-varying sinusoidal forces based on Morison's equation, while triboelectric output power was calculated from rotational velocity and contact-separation cycles derived from multi-body dynamics in MATLAB. This combined approach allows accurate capture of fluid-structure-electrical interactions in the rotor-type TENG system. The specific parameter settings of the rotor nanogenerator are listed in Table 1.

Output power is (30):

$$P_{out} = \frac{1}{2} C_d \rho A v^3 \tag{30}$$

Where, C_d is the drag coefficient, ρ is the density of water, A is the force-receiving area of the structure, and v is the wave velocity. In this simulation, the parameters are set as follows: $C_d = 1.2, \rho = 1025 \text{ kg/m}^3, A = 0.012 \text{ m}^2, v = 0.5 \text{ m/s}$, yielding approximately 32.8 W (consistent with Table 2).

Figure 2 illustrates the comparison of output power between the pre-optimization and post-optimization cases.

Table 1. Parameter settings

Parameter	Value	Unit	Parameter	Value	Unit
Rotor diameter	138	mm	Electrode thickness	4	mm
Rotor thickness	12	mm	Spring constant	420	N/m
Shaft length	180	mm	Damping coefficient	0.05	Ns/m
Rotor blade diameter	60	mm	Electrode spacing	5	mm
Number of blades	5	blade	Electrode stiffness coefficient	150	N/m
Blade angle	52	°	Wave height	50	mm
Blade material	Polymer-based composite material	—	Wave frequency	0.3	Hz
Electrode material	Polymer composite material	—	—	—	—

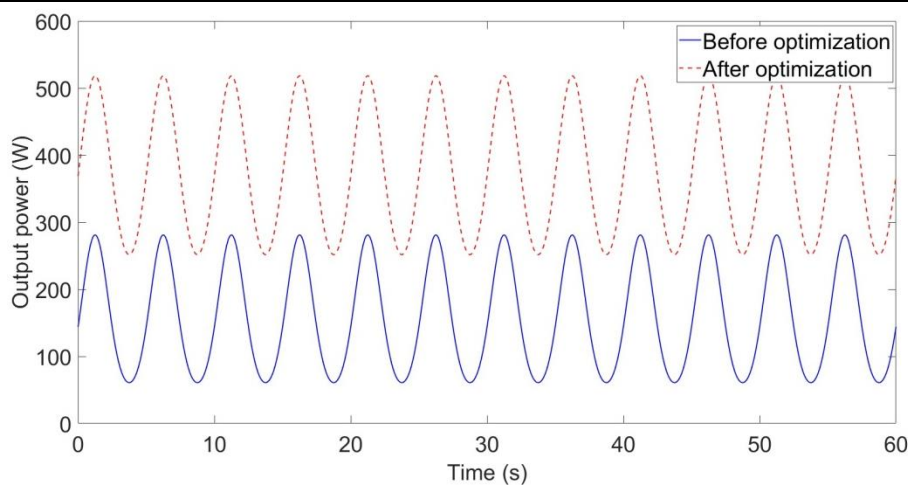


Figure 2. Comparison of output power before and after optimization

The data indicate that under standard wave conditions, the optimized design achieves an average increase of 29.6% in output power, a 15% reduction in fluctuation amplitude, and a 26.7% decrease in the stress at the maximum stress point, effectively mitigating the risk of structural fatigue.

In the simulation, assuming wave velocity $v = 2.5\text{m/s}$, water density $\rho = 1000\text{kg/m}^3$, drag coefficient $C_d = 1.2$, and impact area $A = 0.3\text{m}^2$, the calculation is performed by substituting these values into the formula (31):

$$P_{\text{out}} = \frac{1}{2} \times 1.2 \times 1000 \times 0.3 \times (2.5)^3 = 45.6\text{W} \quad (31)$$

After structural optimization, the increment in power output and the improvement in stability of the rotor-type nanogenerator can be quantified by the following formula (32):

$$P_{\text{opt}} = P_{\text{orig}} \times (1 + \Delta P) \quad (32)$$

Where, P_{opt} represents the power after optimization, P_{orig} represents the power before optimization, and ΔP denotes the percentage improvement in power.

The reduction of stress at the maximum stress point is calculated as (33):

$$\sigma_{\text{opt}} = \sigma_{\text{orig}} \times (1 - \Delta\sigma) \quad (33)$$

Where, σ_{opt} represents the stress after optimization, σ_{orig} represents the stress before optimization, and $\Delta\sigma$ denotes the percentage reduction in stress, as shown in (34).

$$\sigma_{\text{opt}} = 38.5 \times (1 - 0.267) = 28.2\text{MPa} \quad (34)$$

The simulation results indicate that the optimized design significantly enhances the stability of the rotor nanogenerator and increases energy output. In the original design, the system exhibited strong responses to external wave disturbances, particularly under conditions of longer

wave periods, where the generator structure experienced considerable vibrations. This not only affected the continuous energy output but also increased the risk of fatigue during long-term operation. After optimization, the vibration amplitude of the system was effectively reduced. The changes in device vibration before and after optimization are shown in Figure 3.

The comparison results of the simulation analysis before and after optimization are presented in Table 2.

After optimization, the system exhibits more stable operational characteristics, with a particularly significant improvement in the stability of energy output under varying wave conditions. The optimized design substantially reduces the response time of the generator to changes in wave periods, minimizing energy loss caused by fluctuations in wave frequency and effectively enhancing overall energy conversion efficiency. Dynamic response analyses under different wave heights and periods further confirm the adaptability of the optimized design to various marine environments, as shown in (35).

$$E_{\text{opt}} = \frac{P_{\text{max}} \times T_{\text{max}}}{V_{\text{eff}}} \quad (35)$$

Where, $P_{\text{max}} = 43.5\text{W}$ represents the maximum output power, $T_{\text{max}} = 2.5\text{s}$ is the maximum wave period, and $V_{\text{eff}} = 8.5\text{m/s}$ denotes the effective water flow velocity. Calculations show that the energy conversion efficiency E_{opt} after optimization increased by 22%, exhibiting a significant improvement compared with the pre-optimization case. Figure 4 illustrates the trend of power output before and after optimization.

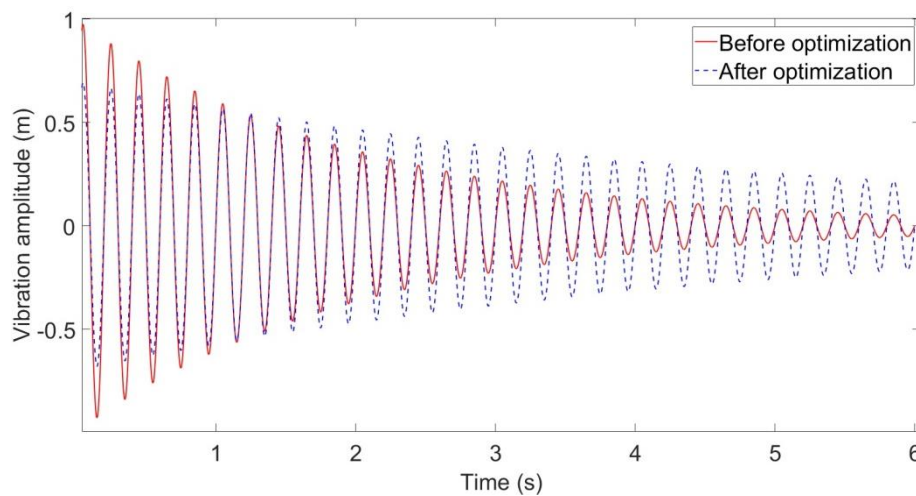


Figure 3. Variation of vibration amplitude before and after optimization

Table 2. Performance comparison before and after optimization

Performance Metric	Baseline Design	Optimized Design	Improvement
Average output power	32.8 W	43.5 W	+32.6%
Power Fluctuation Amplitude	18.9%	15.4%	-18.4%
Maximum Stress	42 MPa	33 MPa	-21%
Maximum Deformation Curvature	0.0075 mm/m	0.0042 mm/m	-44%
Vibration Amplitude	15 mm	10 mm	-33.3%

The optimized results are compared with the experimental results reported in Ref. [32]. In Ref. [32], a wave-driven triboelectric nanogenerator (TENG) was systematically evaluated under various wave conditions by combining a computational fluid dynamics (CFD)-based design approach with experimental validation. Under a wave amplitude of 115 mm and a frequency of 2.2 Hz, the device achieved an output voltage of 133 V; when the excitation frequency was increased to 7 Hz, the output voltage further increased to 333.67 V. In addition, the prototype was able to stably charge a 47 μF capacitor to 0.496 V within one minute, demonstrating effective energy harvesting capability under dynamic wave loads. These results provide an important benchmark for the optimized rotor-type nanogenerator proposed in this study. Under typical wave conditions, the proposed device achieved an average output power of approximately 43.5 W and exhibited significant improvements in operational stability. A direct performance comparison under realistic marine excitations clearly highlights the advantages of structural optimization and multi-objective design approaches in simultaneously enhancing electrical output and mechanical robustness.

4.1. Model Sensitivity Analysis

To evaluate the robustness of the established multi-objective optimization model and the sensitivity of the optimization results to parameter variations, a sensitivity analysis was conducted on key design parameters and external environmental parameters in this study. The sensitivity analysis employed the one-at-a-time (OAT) method, where a single parameter was perturbed by ±20% while keeping all other parameters constant, and the effects on the primary optimization objectives (average output power P_{avg} and maximum equivalent stress σ_{max}) were observed. The selected key parameters include:

Design parameters: rotor diameter D_r , rotor thickness t_r , spring constant k_s , blade angle θ , number of blades N_b ; External environmental parameters: wave height H , wave frequency f_w , wave incidence angle α . The sensitivity index is defined as the relative change rate of the objective function, as shown in (36):

$$S_i = \frac{\Delta O/O_0}{\Delta p_i/p_{i0}} \times 100\% \tag{36}$$

Where O_0 and p_{i0} are the objective function value and parameter value under baseline conditions, and ΔO and Δp_i are the corresponding changes. A larger $|S_i|$ indicates higher sensitivity of the model to that parameter. The sensitivity analysis results are summarized in Table 3.

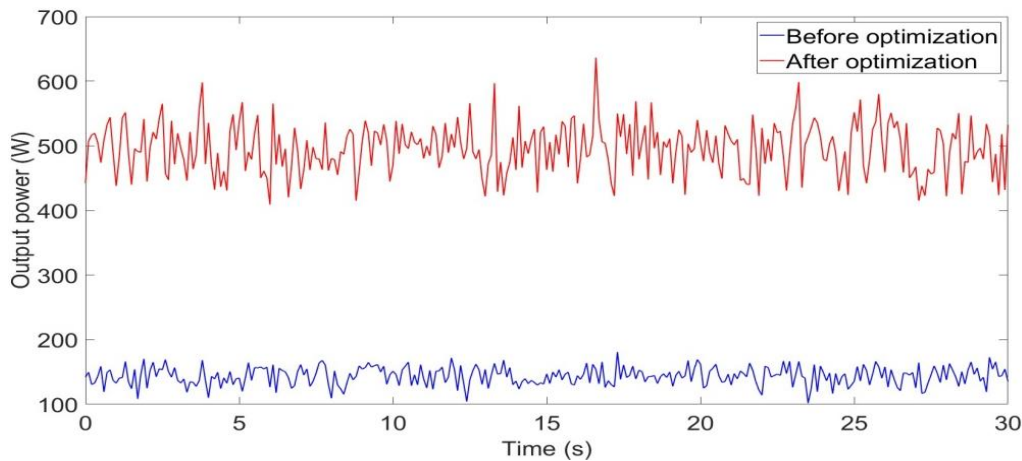


Figure 4. Variation of output power before and after optimization

Table 3 Results of sensitivity analysis for key parameters

Parameter Name	Symbol	Baseline Value	Perturbation Amplitude	Impact on Average Output Power(%)	Impact on Maximum Equivalent Stress(%)	Sensitivity Conclusion
Rotor Diameter	D_r	120 mm	±20%	+18.6/-17.2	-12.4/+14.1	High sensitivity (power-dominant)
Rotor Thickness	t_r	10mm	±20%	+5.3/-4.9	-15.8/+18.3	High sensitivity (stability-dominant)
Spring Constant	k_s	500N/m	±20%	+8.7/-9.1	+11.2/-10.5	Moderate sensitivity
Blade Angle	θ	45°	±20%	+12.4/-11.8	+6.3/-5.9	Moderate sensitivity
Number of Blades	N_b	4	±1	+9.8/-8.5	+4.2/-3.9	Moderate sensitivity
Wave Height	H	50mm	±20%	+21.3/-19.7	+16.8/-15.4	High sensitivity
Wave Frequency	f_w	0.3Hz	±20%	+21.3/-19.7	+9.7 / -8.8	Moderate sensitivity
Wave Incidence Angle	α	0°	±20%	+7.2/-6.8	+5.1/ -4.7	Low sensitivity

The results indicate: The model is most sensitive to rotor diameter and wave height, which is consistent with the direct relationship between output power and wave capture area as well as wave energy density; Rotor thickness has a significant impact on structural stability, with increased thickness effectively reducing maximum stress; Perturbations in external environmental parameters (such as wave height and wave frequency) have substantial effects on both objectives, indicating that the optimized design is effective under typical sea conditions but requires further robust design considerations for extreme conditions; Overall, within the $\pm 20\%$ parameter perturbation range for the optimized model, the average output power fluctuates by no more than 22%, and the maximum equivalent stress fluctuates by no more than 19%, demonstrating good robustness of the optimization results.

In addition, to further verify the stability of the Pareto front, repeated experiments (10 independent runs) were conducted on the convergence of the NSGA-II algorithm under the same parameter perturbations. The results show that the coefficient of variation of the Hypervolume indicator for the Pareto front is less than 5.8%, indicating strong robustness of the algorithm to parameter uncertainties.

The sensitivity analysis results confirm the reliability of the proposed optimization model and results, providing an important reference for design decisions under parameter uncertainties in practical engineering applications.

5. CONCLUSIONS

This work investigates a multi-objective optimization approach for rotor-type triboelectric nanogenerators to improve both energy conversion efficiency and structural reliability in wave energy harvesting. The optimization process accounts for power output, dynamic response, and mechanical constraints, ensuring a balance between efficiency and durability. Simulation analysis confirms that the optimized structure achieves significantly higher power generation with improved stability, effectively mitigating fatigue risks under varying wave periods and amplitudes. The results indicate that the optimized nanogenerator not only delivers stable energy output but also adapts well to diverse marine environments. Compared with the original design, the improved system shortens response time to wave fluctuations and reduces energy losses, achieving a 22% enhancement in conversion efficiency. Overall, the proposed optimization strategy provides a promising solution for the practical deployment of nanogenerator-based wave energy devices, offering a pathway toward sustainable, self-powered systems in real-world ocean conditions.

Funding

This research was funded by Shandong Provincial Natural Science Foundation (Grant No. ZR2024ME241).

Competing Interests

The authors declare no competing interests.

Data Availability Statement

The data used to support the findings of this study are all in the manuscript.

References

- [1] B. Guo and J. Ringwood, "A review of wave energy technology from a research and commercial perspective", *IET Renewable Power Generation*, Vol. 15, No. 14, 2021, pp. 3065-3090. <https://doi.org/10.1049/rpg2.12303>.
- [2] A. F. O. Falcão and J. C. C. Henriques, "Oscillating-water-column wave energy converters and air turbines: A review", *Renewable Energy*, Vol. 85, 2016, pp. 1391-1424. <https://doi.org/10.1016/j.renene.2015.07.086>.
- [3] M. Penalba, J. V. Ringwood, "A review of wave-to-wire models for wave energy converters", *Energies*, Vol. 10, No. 7, 2017, pp. 968. <https://doi.org/10.3390/en10070968>.
- [4] I. López, J. Andreu, S. Ceballos, I. M. De Alegría, I. Kortabarria, "Review of wave energy technologies and the necessary power-equipment", *Renewable and Sustainable Energy Reviews*, Vol. 27, 2013, pp. 413-434. <https://doi.org/10.1016/j.rser.2013.04.016>.
- [5] A. Clément, P. McCullen, A. Falcão, A. Fiorentino, F. Gardner, K. Hammarlund, et al., "Wave energy in Europe: Current status and perspectives", *Renewable and Sustainable Energy Reviews*, Vol. 6, No. 5, 2002, pp. 405-431. [https://doi.org/10.1016/S1364-0321\(02\)00009-6](https://doi.org/10.1016/S1364-0321(02)00009-6).
- [6] G. Lavidas, "Wave energy resource modelling and energy yield: Developments in the past 10 years", *Journal of Ocean Engineering and Marine Energy*, Vol. 9, 2023, pp. 1-22. <https://doi.org/10.1007/s40722-022-00218-9>.
- [7] A. Shadmani, M. R. Nikoo, A. H. Gandomi, "Adaptive systematic optimization of a multi-axis ocean wave energy converter", *Renewable and Sustainable Energy Reviews*, Vol. 189, Part A, 2024, pp. 113915. <https://doi.org/10.1016/j.rser.2023.113915>.
- [8] Z. L. Wang, "Triboelectric nanogenerators as new energy technology for self-powered systems and as active mechanical and chemical sensors", *ACS Nano*, Vol. 7, No. 11, 2013, pp. 9533-9557. <https://doi.org/10.1021/nn404614z>.
- [9] H. Zou, Y. Zhang, L. Guo, P. Wang, X. He, G. Dai, et al., "Quantifying the triboelectric series", *Nature Communications*, Vol. 10, No. 1, 2019, pp. 1427. <https://doi.org/10.1038/s41467-019-09462-z>.
- [10] Y. Lou, M. Li, A. Yu, J. Zhai, Z. L. Wang, "From wave energy to electricity: Functional design and performance analysis of triboelectric nanogenerators", *Nano-Micro Letters*, Vol. 17, No. 1, 2025, pp. 111. <https://doi.org/10.1007/s40820-025-01811-3>.
- [11] C. Rodrigues, D. Nunes, D. Clemente, N. Mathias, J. M. Correia, P. Rosa-Santos, et al., "Emerging triboelectric nanogenerators for ocean wave energy harvesting: State of the art and future perspectives", *Nano Energy*, Vol. 76, 2020, pp. 104981. <https://doi.org/10.1016/j.nanoen.2020.104981>.
- [12] J. He, X. Wang, Y. Nan, H. Zhou, "Research progress of triboelectric nanogenerators for ocean wave energy harvesting", *Small*, Vol. 21, No. 12, 2025, pp. e2411074. <https://doi.org/10.1002/sml.202411074>.
- [13] X. Liang, S. Liu, H. Yang, T. Jiang, "Triboelectric nanogenerators for ocean wave energy harvesting: Unit integration and network construction", *Electronics*, Vol. 12, No. 1, 2023, pp. 225. <https://doi.org/10.3390/electronics12010225>.
- [14] Y. Feng, T. Jiang, X. Liang, J. An, Z. L. Wang, "Cylindrical triboelectric nanogenerator based on swing structure for efficient harvesting of ultra-low-frequency water wave energy", *Applied Physics Reviews*, Vol. 9, No. 1, 2022, pp. 011413. <https://doi.org/10.1063/5.0077569>.

- [15] C Zhang, W Yuan, B Zhang, J Yang, Y Hu, L He, et al., "A rotating triboelectric nanogenerator driven by bidirectional swing for water wave energy harvesting", *Small*, Vol. 19, No. 50, 2023, pp. e2304412. <https://doi.org/10.1002/sml.202304412>.
- [16] D Zhao, H Li, Y Yu, Y Wang, J Wang, Q Gao, et al., "A current-enhanced triboelectric nanogenerator with crossed rollers for harvesting wave energy", *Nano Energy*, Vol. 115, 2023, pp. 108739. <https://doi.org/10.1016/j.nanoen.2023.108739>.
- [17] C Wu, R Liu, J Wang, Y Zi, L Lin, ZL Wang, "A spring-based resonance coupling for hugely enhancing the performance of triboelectric nanogenerators for harvesting low-frequency vibration energy", *Nano Energy*, Vol. 32, 2017, pp. 287-293. <https://doi.org/10.1016/j.nanoen.2016.12.043>.
- [18] Y Pang, S Chen, Y Chu, ZL Wang, C Cao, "Matryoshka-inspired hierarchically structured triboelectric nanogenerators for wave energy harvesting", *Nano Energy*, Vol. 66, 2019, pp. 104131. <https://doi.org/10.1016/j.nanoen.2019.104131>.
- [19] A Shadmani, MR Nikoo, AH Gandomi, M Chen, R Nazari, "Advancements in optimizing wave energy converter geometry utilizing metaheuristic algorithms", *Renewable and Sustainable Energy Reviews*, Vol. 197, 2024, pp. 114404. <https://doi.org/10.1016/j.rser.2024.114404>.
- [20] G. Giorgi and M. Bonfanti, "Optimization and energy maximizing control systems for wave energy converters II", *Journal of Marine Science and Engineering*, Vol. 12, No. 8, 2024, pp. 1297. <https://doi.org/10.3390/jmse12081297>.
- [21] A Cotten, DIM Forehand, "Multi-objective optimisation of a sloped-motion, multibody wave energy converter concept", *Renewable Energy*, Vol. 194, 2022, pp. 307-320. <https://doi.org/10.1016/j.renene.2022.05.098>.
- [22] MMH Karani, MR Nikoo, HD Pirooz, A Shadmani, S Al-Saadi, AH Gandomi, "Multi-objective evolutionary framework for layout and operational optimization of a multi-body wave energy converter", *Energy*, Vol. 313, 2024, pp. 130054. <https://doi.org/10.1016/j.energy.2024.130054>.
- [23] A. Meduri and H. Kang, "Synergistic integration of multiple wave energy converters with adaptive resonance and offshore floating wind turbines through Bayesian optimization", *Journal of Marine Science and Engineering*, Vol. 12, No. 8, 2024, pp. 1455. <https://doi.org/10.3390/jmse12081455>.
- [24] A Garcia-Teruel, B DuPont, DIM Forehand, "Hull geometry optimisation of wave energy converters: On the choice of the objective functions and the optimisation formulation", *Applied Energy*, Vol. 298, 2021, pp. 117153. <https://doi.org/10.1016/j.apenergy.2021.117153>.
- [25] K Khanal, N DeGoede, O Vitale, MN Haji, "Multi-objective multidisciplinary optimization of wave energy converter array layout and controls", *Renewable Energy*, Vol. 225, 2024, pp. 120289. <https://doi.org/10.1016/j.renene.2024.120289>.
- [26] M Yuan, W Yu, Y Jiang, Z Ding, Z Zhang, X Zhang, et al., "Triboelectric nanogenerator metamaterials for joint structural vibration mitigation and self-powered structure monitoring", *Nano Energy*, Vol. 104, Part A, 2022, pp. 107896. <https://doi.org/10.1016/j.nanoen.2022.107896>.
- [27] A. F. O. Falcão, "Wave energy utilization: A review of the technologies", *Renewable and Sustainable Energy Reviews*, Vol. 14, No. 3, 2010, pp. 899-918. <https://doi.org/10.1016/j.rser.2009.11.003>.
- [28] J. Falnes, "A review of wave-energy extraction", *Marine Structures*, Vol. 20, No. 4, 2007, pp. 185-201. <https://doi.org/10.1016/j.marstruc.2007.09.001>.
- [29] C. Guedes Soares, "Fatigue design of marine structures", in *Fatigue Design of Marine Structures*, Cambridge University Press, 2016, pp. 1-28. <https://doi.org/10.1017/CBO9781316271643>.
- [30] P. R. Thies, L. Johanning, and G. H. Smith, "Assessing mechanical loading regimes and fatigue life of marine power cables in marine energy applications", *Proceedings of the Institution of Mechanical Engineers, Part O: Journal of Risk and Reliability*, Vol. 226, No. 5, 2012, pp. 467-480. <https://doi.org/10.1177/1748006X11413533>.
- [31] J He, X Zheng, Z Zheng, D Kong, K Ding, N Chen, et al., "Advances in triboelectric nanogenerators based on polymer composites", *Nano Energy*, Vol. 92, 2022, pp. 106748. <https://doi.org/10.1016/j.nanoen.2021.106748>.
- [32] Y Wang, ATT Pham, X Han, D Du, Y Tang, "Design and evaluate the wave driven-triboelectric nanogenerator under external wave parameters: Experiment and simulation", *Nano Energy*, Vol. 93, 2022, Article No. 106844. <https://doi.org/10.1016/j.nanoen.2021.106844>.

